

# Efficacious Removal of Trace Mercury from Honeysuckle Water Decoction Using Multifunctional Mesoporous Carbon

Wenjie Lu, Yiqian Ma, Huanyu Lu, Xiaoyan Yuan, Jianyong Zhang,\* and Ming Yu\*

Cite This: *ACS Omega* 2022, 7, 46787–46797

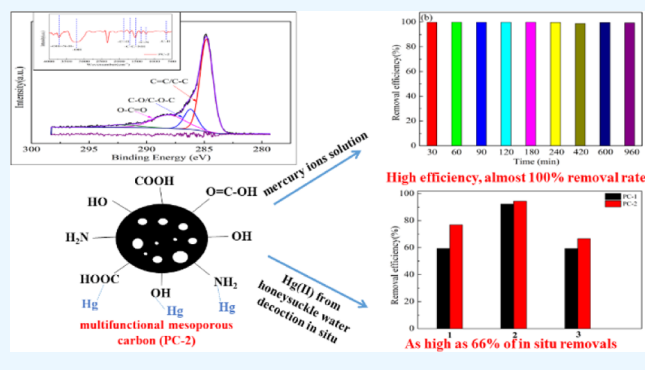
Read Online

ACCESS |

Metrics &amp; More

Article Recommendations

**ABSTRACT:** A mesoporous carbon (PC-2) obtained by using sucrose as a carbon source and urea as a nitrogen source has been used to remove trace mercury (Hg) from honeysuckle water decoction with high efficiency. The morphology, chemical composition, and pore structure of PC-2 have been characterized by scanning electron microscopy (SEM), Fourier transform infrared spectroscopy (FT-IR), and Brunauer–Emmett–Teller (BET). The results show that the specific surface area of PC-2 with the  $-\text{NH}_2$  functional is  $1077.44 \text{ m}^2 \cdot \text{g}^{-1}$ , and the mesoporous pore size is mainly around 2.8 nm. The investigation of the relationship between the adsorption performance and the structure of PC-2 indicates that the pore size and the chemical composition of carbons are significantly correlated with adsorption performance of mercury in water and honeysuckle water decoction. PC-2 has high efficiency approximated 100% for mercury from aqueous solutions. The pseudo-second-order kinetic model and the Freundlich model could better fit the adsorption process of Hg(II) onto PC-2. The process was dominated by chemical adsorption. Meanwhile, the adsorption behavior and the influence on the medicinal components (chlorogenic acid) of mercury removal in honeysuckle water decoction were determined by high performance liquid chromatography (HPLC). Results suggest that PC-2 has high efficiency approximated 66% for mercury from honeysuckle water decoction under optimal adsorption conditions, without affecting its active ingredients (chlorogenic acid). Therefore, PC-2 can potentially be used for adsorption of mercury in honeysuckle water decoction.



## 1. INTRODUCTION

Traditional Chinese medicine (TCM) has been widely applied to prevent and cure diseases. However, the presence of heavy metals in Chinese herbs seriously prohibits the widespread use of TCM, due to its high toxicity, persistence, bioaccumulation, and long distance transmission.<sup>1–3</sup> Mercury is considered as one of the most toxic heavy metals, when the cumulative content of mercury in the blood exceeds  $200 \text{ g} \cdot \text{L}^{-1}$ ; it may directly damage the human central nervous system, resulting in hearing impairment, loss of speech, tetraplegia, and even dementia.<sup>4</sup> Therefore, trace heavy metal in TCM is dangerous to human health. In recent years, there have been many research studies focusing on the removal of heavy metals in simulated Chinese herbal medicines (CHMs), while less attention has been paid to the in situ removal of trace heavy metals from CHMs.<sup>5–7</sup> Therefore, it is of great importance to develop a highly active method for in situ removal of heavy metals from herbal water decoction.

Honeysuckle, a traditional CHM, has various pharmacological activities such as antibacterial, antiviral, and immunity enhancing. It is extensively used for the treatment of sore throat, anemofrigid cold, and so on.<sup>8,9</sup> Chlorogenic acid, one of the main active components of honeysuckle, has significant

biological activities such as anti-inflammation, antioxidant, and anti-tumor.<sup>10–12</sup> Chinese Pharmacopoeia stipulates that its content is one of the most important indicators for quality control of honeysuckle. Guo et al.<sup>13</sup> have studied the content of four heavy metals (Pb, As, Hg, and Cd) in different categories of Chinese herbs, indicating that heavy metal content in honeysuckle was without the limitation of quantity. Consequently, the regulation of heavy metals from honeysuckle before its application in the clinic helps to ensure the safety of medication. At present, methods of removing heavy metals in simulated CHMs mainly include flocculation precipitation,<sup>14</sup> adsorption method,<sup>15</sup> molecular sieve,<sup>16</sup> micro-organism method,<sup>17</sup> nanotechnology, and molecular/ion imprinting technology.<sup>18–20</sup> Adsorption has a social and economy of advantage over other methods, ascribable to its

Received: September 9, 2022

Accepted: November 25, 2022

Published: December 5, 2022



high efficiency, economy, and high feasibility. Adsorbents for removing heavy metals from CHMs are mainly chelating resin,  $\gamma$ -mercaptopropyl/allylthiourea silica gel,<sup>21,22</sup> chitosan,<sup>23</sup> activated carbon,<sup>24</sup> and bionic materials.<sup>25</sup> High absorption efficiency of heavy metals in CHMs is caused by intermolecular chemical bonding, van der Waals forces, or material capture ability to adsorb heavy metal ions. The key to high absorption efficiency of heavy metals in CHMs is to remove heavy metals, while ensuring that the amount of active ingredients is not reduced. Although these methods focus upon the changes of the components of CHMs in the removal of heavy metals, studies have seldom been carried out on the effects of trace heavy metals in CHMs on the quality control of TCM and human health.

Mesoporous carbon has been attracting a lot of interest in removing heavy metals from wastewater due to its large specific surface area, feasible pore, modifiable surface active spots, good hydrothermal stability, and so on.<sup>26,27</sup> Lian et al.<sup>28</sup> applied mesoporous carbon to the removal of heavy metals from water, which showed a high adsorption performance. However, herbal water decoction is a heterogeneous mixture of pharmacodynamic components. The existing mesoporous carbon is not sufficient as adsorbent for trace heavy metals from herbal water decoction. In addition, the existence of micro-trace heavy metals in Chinese herbal medicines are difficult to degrade and threaten human health.<sup>29,30</sup> Therefore, it is essential to develop a proper treatment of trace heavy metals from herbal water decoction, without affecting the active components. The goal of this study is to establish the mesoporous carbon for effective removal of trace mercury from honeysuckle water decoction and maintain the concentration of active components of honeysuckle. The mechanism of adsorption of mercury on the obtained mesoporous carbon is explained by adsorption kinetics and adsorption isotherm model.

## 2. RESULTS AND DISCUSSION

### 2.1. Characterization of Prepared Mesoporous Carbons.

Figures 1a–d and 2 show the micromorphology of PC-1 and PC-2. As shown in Figure 1a, the micromorphology of PC-1 is petal-like lamellae and with a large number of pores. The TEM image (Figure 2) confirms that there are many micro

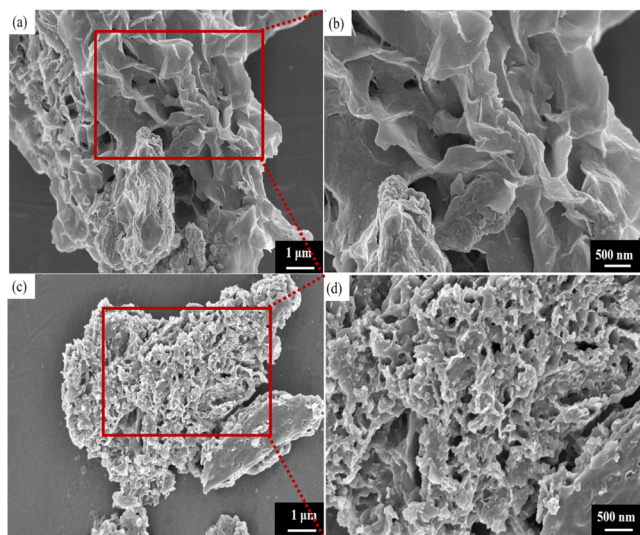


Figure 1. SEM images: (a,b) PC-1 and (c,d) PC-2.

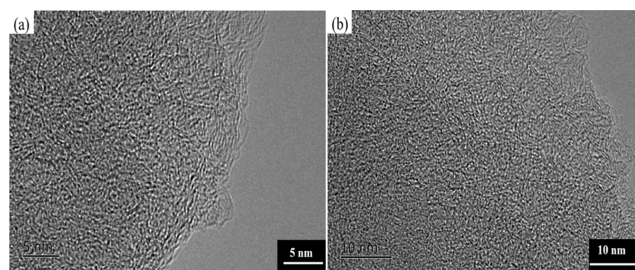


Figure 2. TEM images: (a,b) PC-1.

pores for PC-1. It can be seen from Figure 1c,d that there are lots of irregular pores on the surface of PC-2 carbon particles, and more and more uniform holes are distributed on the carbon particles. This proves that PC-1 and PC-2 have different pore structures that have been fabricated by different methods.

The chemical compositions of PC-1 and PC-2 are analyzed by FT-IR and XPS. Figure 3 shows the FT-IR spectra of PC-1

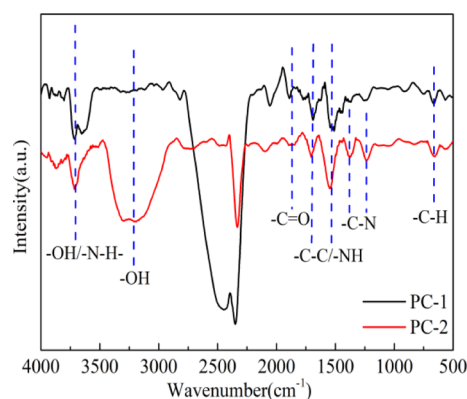
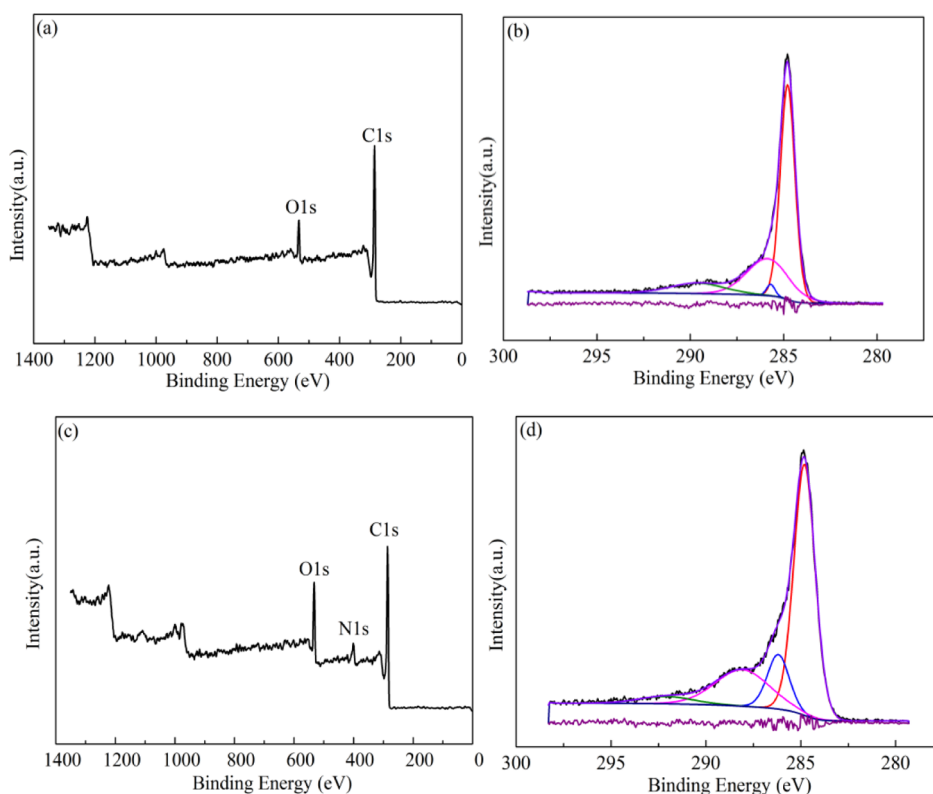


Figure 3. FT-IR spectra.

and PC-2. It can be observed from Figure 3 that the adsorption peaks of PC-1 mainly appeared near 3714, 2822, 2057 and 1885, 1691 and 1521, 1244, and 661  $\text{cm}^{-1}$ , which were attributed to the O–H vibration,  $\text{CH}_3$  vibration,  $\text{C}=\text{O}$  vibration, benzene skeletal vibration,  $\text{C}-\text{O}-\text{C}/\text{C}-\text{C}$  stretching vibration, and C–H bending vibration, respectively.<sup>31,32</sup> PC-2 shows major adsorption peaks at 3869 and 3718, 3248, 2090 and 1701, 1543, 1369 and 1228, and 654  $\text{cm}^{-1}$ , corresponding to the stretching vibration of the N–H, O–H,  $\text{C}=\text{O}$ , N–H bending vibration/ $\text{C}=\text{C}$  stretching vibration, and stretching vibration of the C–N and C–H bending vibrations, respectively.<sup>33–35</sup> The FT-IR spectra of PC-2 show two absorption peaks N–H and C–N compared to PC-1. This also proves that the addition of urea enables nitrogen doping on the surface of mesoporous carbon (PC-2).

The types and contents of the functional groups are investigated via XPS to confirm the difference of chemical composition in the PC-1 and PC-2. Figure 4a,c shows the binding energy spectra of PC-1 and PC-2, respectively. The results show that PC-1 consisted of intense C 1s (284.7 eV) and O 1s (532.3 eV), while PC-2 contained three peaks of C 1s (284.7 eV), N 1s (400.0 eV), and O 1s (532.3 eV). The high-resolution C 1s XPS spectra of PC-1 and PC-2 are compared in Figure 4b,d. The C 1s peaks<sup>36</sup> for PC-1 in Figure 4b corresponded to the  $\text{C}=\text{C}/\text{C}-\text{C}$  (284.79 eV), C–H (285.69 eV), C–O (285.86 eV), O–C=O (289.61 eV), and



**Figure 4.** (a) XPS survey-scan spectra for PC-1; (b) C 1s XPS spectra for PC-1; (c) XPS survey-scan spectra for PC-2; (d) C 1s XPS spectra for PC-2.

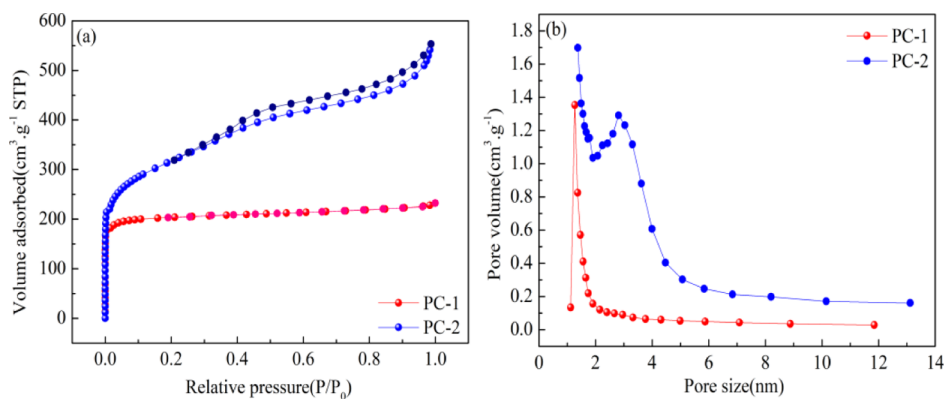


**Figure 5.**  $N_2$  adsorption–desorption isotherms (a) and pore size distribution curves (b) of PC-1 and PC-2.

C=C/C–C and C–O bond, which were dominated by the 51.48 and 25.33% content; the O–H peak at 532.8 eV accounted for 9.85% for PC-1. The C 1s peaks for PC-2 shown in Figure 4d corresponded to C=C/C–C (284.81 eV), O–C=O (288.08 eV), C–O/C–O–C (286.19 eV), and C=C/C–C and O–C=O bond, which were dominated by the 51.48 and 25.33% content; the O–H peak at 532.4 eV accounted for 15.18%. The combined FT-IR and XPS analysis suggests that PC-1 mainly contains functional groups of O–H and COOH, and PC-2 is with functional groups such as O–H, COOH, and  $NH_2$ . Moreover, PC-2 has a richer functional group structure than PC-1 and is rich in  $-NH_2$ , which can provide more active sites for mercury adsorption.

The pore structures of PC-1 and PC-2 are further investigated by the  $N_2$  adsorption–desorption isotherm. It can be seen in Figure 5a that the isotherm of PC-1 was a

typical type I isotherm.<sup>37</sup> As seen in Figure 5a, the absorbed volume of  $N_2$  showed a rapid increase at  $P/P_0$  below to 0.1, indicating that a large number of microporous structures are present in the PC-1. However, the isotherm of PC-1 became very slow at  $P/P_0$  close to 0.2–0.8, indicating that PC-1 consists of few mesoporous features. The pores are primary distributed near 1.2 nm and small 2.2 nm mesopores in PC-1, as observed in Figure 5b. The isotherm (Figure 5a) of PC-2 exhibited a typical type IV based on IUPAC classification,<sup>38</sup> and PC-2 represented a hysteresis loop similar to that of  $H_2$  (b) at  $P/P_0$  near to 0.4–0.9, manifesting that PC-2 consists of dominant mesoporous pores. The pore size distribution (seen in Figure 5b) shows that the pore size of PC-2 was mainly distributed near 2.8 nm, which confirms the existence of mesoporous pores. The results suggest that PC-1 is mainly composed of micropores and few mesopores; PC-2 is mainly

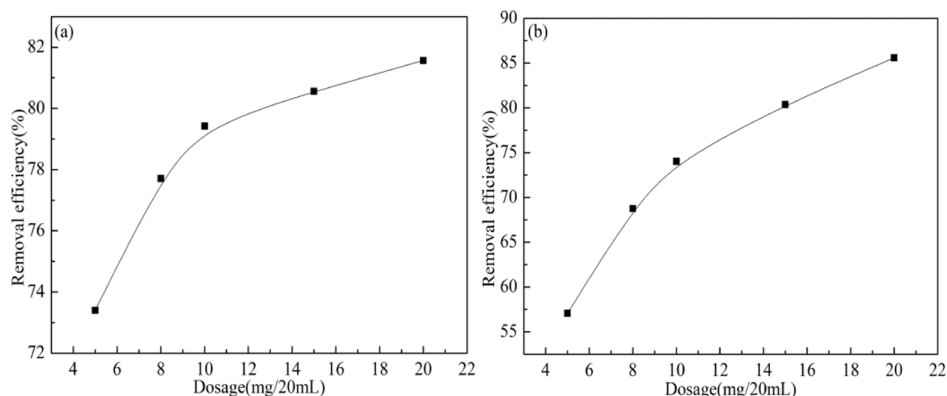


**Figure 6.** Removal rate of heavy metal Hg(II) of different amounts of PC-1 (a) and PC-2 (b).

composed of mesopores and some micropores, which is in full agreement with the results of TEM and SEM analysis.

## 2.2. Study on the Adsorption Properties of Mesoporous Carbon. 2.2.1. Effects of Dosages on Adsorption.

The effect of the adsorbent dose on the removal efficiency of Hg are evaluated in Figure 6. The removal efficiencies of the PC-1 and PC-2 increased from the initial dose of 5 mg/20 mL to a dose of 20 mg/20 mL (10 mg·L<sup>-1</sup> Hg), with 24 h of the adsorption time and a temperature of 30 °C. Figure 6a,b shows that the removal rate of Hg by PC-1 and PC-2 increased gradually with the gradual rise of PC-1 and PC-2 dosage, which may be due to the greater concentration gradient of the surface active adsorption sites on the PC-1 and PC-2. However, compared with PC-1, PC-2 exhibited a higher removal rate, which is because PC-2 has a higher specific surface area and pore volume (Table 1) and richer functional group structure

**Table 1. Structural Parameters of Mesoporous Carbon**

samples	$S_{\text{BET}}$ (m <sup>2</sup> ·g <sup>-1</sup> )	$V_{\text{total}}$ (cm <sup>3</sup> ·g <sup>-1</sup> )	$V_{\text{mic}}$ (cm <sup>3</sup> ·g <sup>-1</sup> )	$V_{\text{meso}}$ (cm <sup>3</sup> ·g <sup>-1</sup> )	$D_{\text{BJH}}$ (nm)
PC-1	656.03	0.376	0.3258	0.0502	2.290
PC-2	1077.44	0.802	0.4661	0.3359	2.977

(Figure 3), promoting the driving force for mass transfer process. Considering the removal rate and economy, 5 mg was chosen as the optimal dose for subsequent low-concentration Hg adsorption experiments.

2.2.2. Effects of Initial Concentration on Adsorption. The effect of different initial concentrations on the Hg adsorption is

presented in Figure 7 (5 mg of adsorbent amount, Hg (II) initial concentration of 0.01, 0.13, 0.16, 0.19, 0.22, 0.30, and 0.40 mg·L<sup>-1</sup>). As seen from Figure 7a,b, the removal rate of Hg by samples PC-1 and PC-2 with the increase of the initial concentration of Hg showed a general trend of increasing first and then leveling off, and the removal rate could reach a high level at the beginning, because PC-1 and PC-2 have numerous active adsorption sites necessary for the adsorption of Hg at the beginning, and the content of Hg in the solution is less. This may be due to the fact that at the beginning, PC-1 and PC-2 have a large number of active adsorption sites necessary for Hg adsorption and less content of Hg in the solution, so the removal rate is high. Afterward, with the further increase of Hg concentration, the removal rate of PC-1 and PC-2 remained basically unchanged, which may be due to the fact that with the increase of Hg concentration, the active adsorption sites on the surface of the material are gradually occupied, the concentration difference between inside and outside the adsorbent decreases, and the adsorption gradually slows down and finally reaches saturation.<sup>39</sup> Therefore, given the high removal rate, the concentration of the optimal Hg solution was 0.22 mg·L<sup>-1</sup>.

2.2.3. Effects of Initial pH on Adsorption. The pH of the solution affects not only the existing form of Hg in the solution, but also the form of surface charge and functional groups of the material in the solution. The mercury ion concentration is 0.22 mg·L<sup>-1</sup> (20 mL), and the pH value at which the mercury ion begins to precipitate at this concentration is around 9.8. As a result, this experiment's pH range is designated as 2–9. Figure 8a shows that the

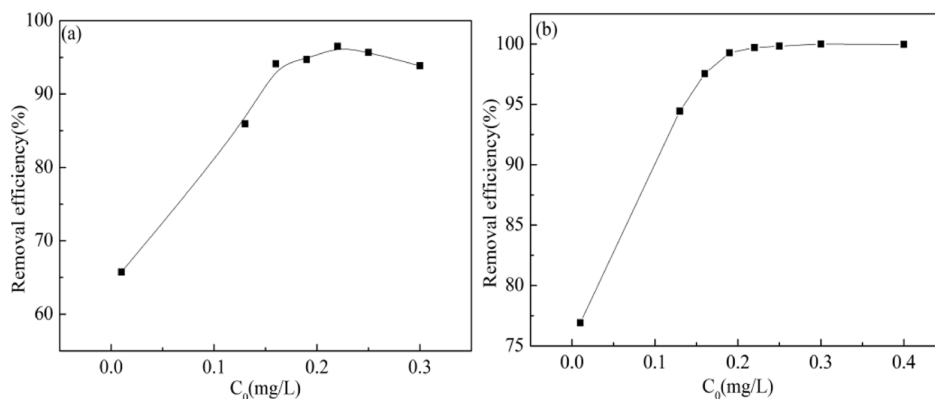


**Figure 7.** Removal efficiency for different concentrations of mercury ions: (a) PC-1 and (b) PC-2.

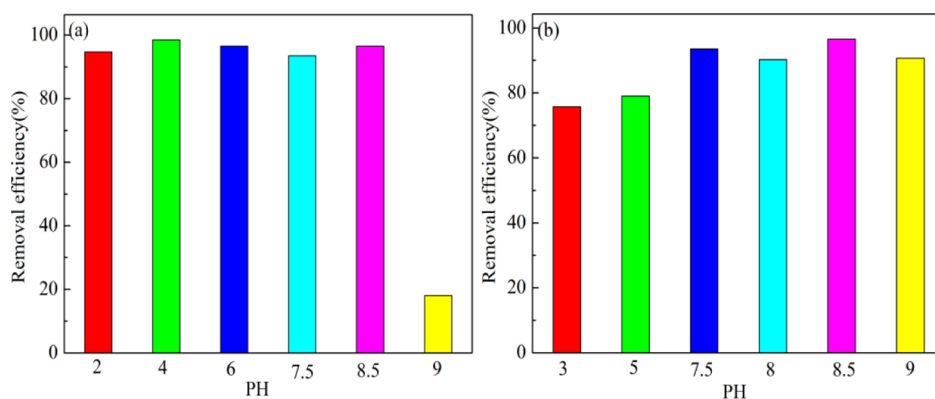


Figure 8. Removal rate of mercury ions at different solutions of pH value: (a) PC-1 and (b) PC-2.

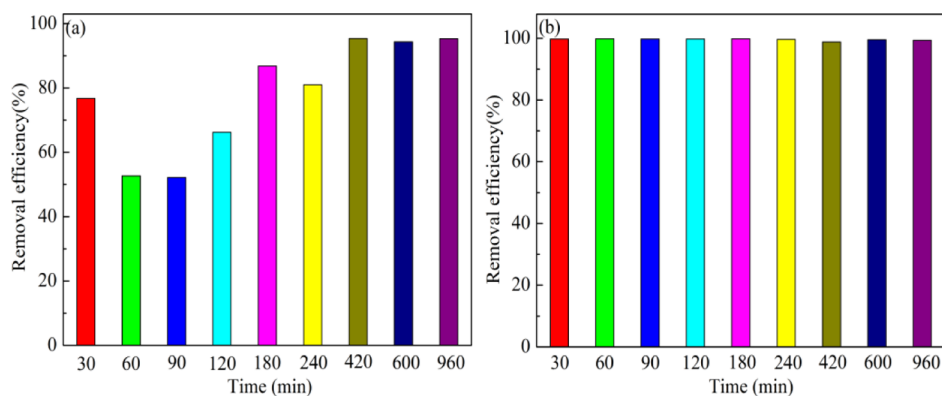


Figure 9. Removal rate of mercury ions at different times: (a) PC-1 and (b) PC-2.

adsorption rate of Hg by PC-1 tended to be flat as the pH fluctuated from 2 to 8.5 and the removal rate decreased rapidly when pH > 8.5, which could be because as the pH rose, Hg could form mercury hydroxide precipitates attached to the surface of the material, obstructing the removal of Hg by PC-1 or the oxygen-containing functional groups (hydroxyl, carboxyl) in PC-1.<sup>40</sup> Figure 8a shows that the removal rate of Hg by sample PC-2 was lower at lower pH and gradually increased when pH > 5, which may be due to the surface  $-\text{COO}^-$  and  $-\text{NH}_2$  of PC-2 being protonated at lower pH and the adsorbent being positively charged, which hindered interaction with the also positively charged  $\text{Hg}^{2+}$ , resulting in a low removal rate, and when pH was higher, more OH, COOH, and  $\text{NH}_3^+$  deprotonated and adsorbent tended to be more negatively charged, which favored the interaction with positively charged  $\text{Hg}^{2+}$ , resulting in an increased removal rate.<sup>41,42</sup> To summarize, PC-1 is within the examined pH range, with an ideal initial pH of 4–8.5, and PC-2 is also within the investigated pH range, with an optimal initial pH of 7.5–9. This study investigated the following variables at pH 7 and 8.5 to permit additional analysis and exploration.

#### 2.2.4. Effects of Different Contact Times on Adsorption.

The adsorption time is one of the main factors to measure the adsorption efficiency. The experimental conditions are as follows: 0.22  $\text{mg}\cdot\text{L}^{-1}$  of mercury ion concentration; 30, 60, 90, 120, 180, 240, 420, 600, and 960 min of adsorption times. The experimental results are shown in Figure 9. Figure 9a,b shows that with the gradual increase of time, the removal rate of Hg by samples PC-1 and PC-2 showed a trend of rising at first and then gradually decreasing until the adsorption equilibrium. However, the removal rate of Hg by PC-1 basically remained

unchanged from 420 min, while the adsorption of Hg by PC-2 basically reached equilibrium at about 30 min, and the removal rate remained unchanged. Obviously, PC-2 has a faster adsorption rate and a higher removal rate, which may be due to the rich micro-mesoporous structure of PC-2 compared with PC-1. It is conducive to the rapid entry of mercury into the pores to occupy more adsorption sites, and hydroxyl groups on the surface, carboxyl, and amino groups are the binding sites of heavy metals,<sup>43</sup> which can undergo ion exchange or complexation with mercury, thereby shortening the adsorption equilibrium time and improving the removal rate. In summary, considering the change trend of removal rate, the optimal adsorption times of PC-1 and PC-2 were 420 and 30 min, respectively.

To further investigate the adsorption process of Hg by PC-1 and PC-2, the pseudo-first-order and the pseudo-second-order models were used to describe the adsorption kinetics of PC-1 and PC-2.

$$\begin{aligned} \text{Pseudo-first-order equation: } & \log(q_e - q_t) \\ & = \log q_e - K_1 t / 2.303 \end{aligned} \quad (1)$$

$$\text{Pseudo-second-order equation: } t/q_t = 1/q_e^2 k_2 + t/q_e \quad (2)$$

where  $k_1$  (1/min) and  $k_2$  ( $\text{g}/(\text{mg}\cdot\text{min})$ ) were the pseudo-first-order and the pseudo-second-order rate constants of sorption, respectively.  $q_t$  ( $\text{mg}/\text{g}$ ) and  $q_e$  ( $\text{mg}/\text{g}$ ) were the amount of adsorbed mercury ions at time  $t$  (h) and the equilibrium sorption capacity, respectively. The kinetic models were

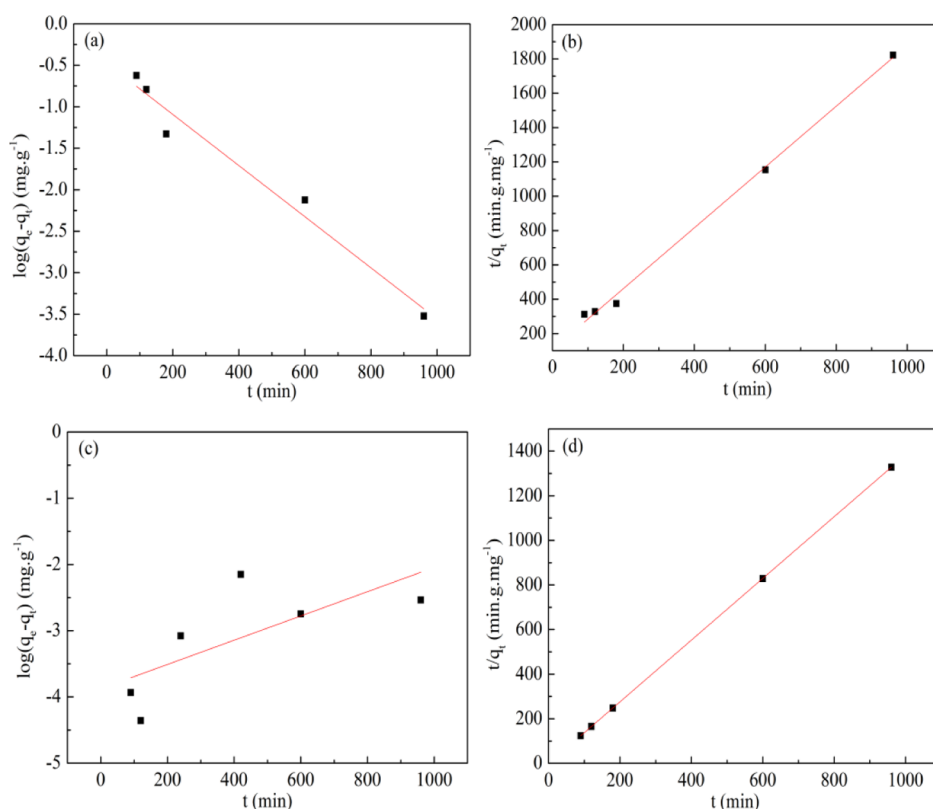


**Figure 10.** Line kinetic plot for the Hg adsorption via the pseudo-first-order model and the pseudo-second-order model for PC-1 and PC-2: (a,b) PC-1 and (c,d) PC-2.

**Table 2.** Kinetic Parameters of the Pseudo-Second-Order and the Pseudo-First-Order Models of PC-1 and PC-2 for Hg

kinetic models	$q_{e,exp}$ (mg/g)	pseudo-first-order			pseudo-second-order		
		$q_e$ (mg/g)	$K_1$ (1/min)	$R^2$	$q_e$ (mg/g)	$K_2$ (g/(mg·min))	$R^2$
PC-1	0.5272	0.3342	0.0069	0.9633	0.5645	0.0292	0.9962
PC-2	0.7262	0.0001	2.3072	0.3918	0.7227	-2.1415	0.9999

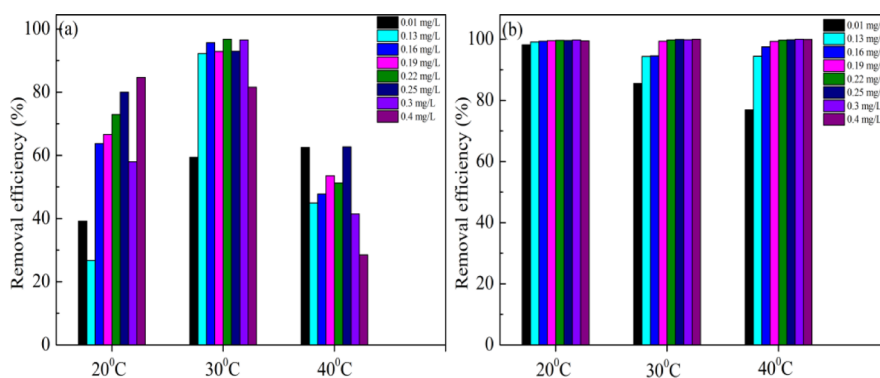


**Figure 11.** Removal rate of mercury ions at different temperatures: (a) PC-1 and (b) PC-2.

applied to fit the experimental data; see Figure 10 and Table 2 for detailed results.

Table 2 shows that the correlation coefficients  $R^2$  of the pseudo-second-order models for both samples were above 0.99 and greater than those of their pseudo-first-order kinetic models. Moreover, the theoretical adsorption amounts ( $q_e$ ) calculated from the pseudo-second-order equation were closer to the actual adsorption amounts, indicating that the Hg adsorption processes of PC-1 and PC-2 could be better described by the pseudo-second-order kinetic models, which

also implies that the adsorption rates of both were mainly dominated by chemisorption.<sup>44</sup>

**2.2.5. Effects of Temperatures on Adsorption.** This work is designed to add 5 mg of PC-1 or PC-2 to 20 mL of different concentrations (0.01, 0.13, 0.16, 0.19, 0.22, 0.30, and 0.40 mg·L<sup>-1</sup>) in Hg solution for adsorption experiments. The results are shown in Figure 11. From Figure 11a, it can be seen that the mercury removal rate of PC-1 showed a general trend of rising and then decreasing with the increase of temperature, and the removal rate of Hg by PC-1 was generally higher at 30 °C, but

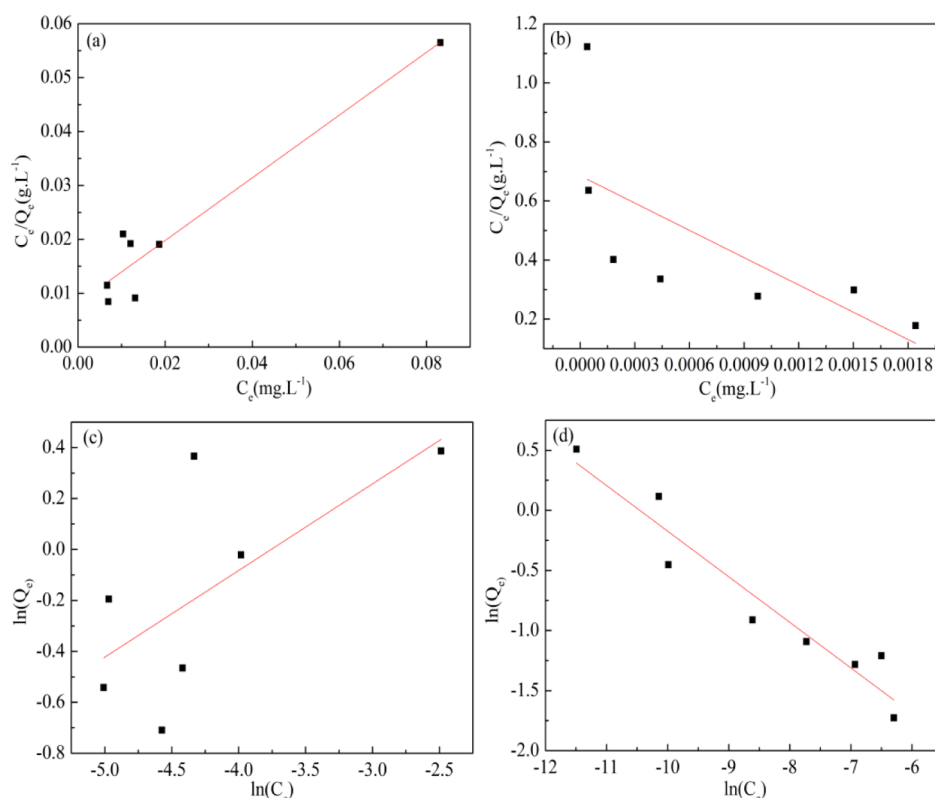


Figure 12. Langmuir and Freundlich isotherm equation simulation curve of PC-1 and PC-2: (a,c) PC-1 and (b,d) PC-2.

Table 3. Parameters for the Langmuir and the Freundlich Models of PC-1 and PC-2 for Hg

samples	Langmuir model			Freundlich model		
	$Q_{\max}$ (mg/g)	$K_L$ (L/mg)	$R^2$	$K_F$ (mg/g) (L/mg) $^{1/n}$	$n$	$R^2$
PC-1	1.7182	72.7506	0.9116	3.5880	2.9412	0.3391
PC-2	0.0032	455.8317	0.3850	0.01895	2.6364	0.9123

the higher the temperature was, the lower was the removal rate. This suggests that increase of temperature had an effect on the stability of mercury, thereby affecting the removal rate. In Figure 11b, with the increasing temperature, the removal rate of Hg at different concentrations of PC-2 did not change significantly, and the removal rate was almost 100%, which indicates that the temperature had little effect on the adsorption performance of PC-2, which may be determined by the special physical properties of the PC-2. In a certain water environment, the sample PC-2 has a certain hydrothermal stability, and its pore size, specific surface area, and pore volume do not change obviously with the change of temperature, so the removal rate of Hg by sample PC-2 at different temperatures is basically unchanged when other conditions remain unchanged. Considering the higher removal rate of mesoporous carbon per unit mass, the best reaction temperature was selected as 30 °C.

In order to deeply investigate the adsorption mechanism of mesoporous carbon on Hg, the Freundlich and the Langmuir adsorption models were used to analyze the equilibrium data of Hg onto PC-1 and PC-2 at the optimum temperature of 30 °C.

$$\text{Langmuir: } C_e/Q_e = 1/Q_{\max}K_L + C_e/Q_{\max} \quad (3)$$

$$\text{Freundlich: } \ln Q_e = 1/n \ln C_e + \ln K_F \quad (4)$$

where  $C_e$  (mg/L) and  $Q_e$  (mg/g) represented the equilibrium concentration of Hg and the adsorption amount of Hg after adsorption equilibrium.  $Q_{\max}$  (mg/g) was the maximum adsorption capacity of PC-1 and PC-2, and  $K_L$  (L/mg) was a Langmuir constant, relating to surface adsorption energy.  $K_F$  (mg/g) (L/mg) $^{1/n}$  was the Freundlich constants related to the sorption capacity and  $n$  represented the sorption intensity. See Figure 12 and Table 3 for the fitting curve and parameters.

From Table 3, it can be concluded that the adsorption of Hg by PC-1 was better described by the Langmuir isotherm model via comparing the correlation coefficients  $R^2$  of the two model fits, while the adsorption of Hg by PC-2 was well described by the Freundlich isotherm model, which implies that the adsorption process of PC-1 was unimolecular layer adsorption and the adsorption process of PC-2 was polymolecular layer adsorption. The Freundlich constant ( $n$ ) in the PC-2 was greater than 1, which indicates that the adsorption of mercury by PC-2 was easy, and it was the preferential adsorption.<sup>45,46</sup>

**2.3. Analysis of Mesoporous Carbon for In Situ Removal of Mercury in Honeysuckle.** In this experiment, the Hg contained in the honeysuckle purchased in the laboratory was measured; we found that it contains a trace amount of mercury, and its content is about 0.009–0.011 mg·kg<sup>-1</sup>. Therefore, samples PC-1 and PC-2 were taken to adsorb in situ mercury in the honeysuckle water decoction under the abovementioned optimal conditions, and the results are shown

in Figure 13. Figure 13 shows that when the Hg concentration in the honeysuckle water decoction was  $0.006 \text{ mg}\cdot\text{L}^{-1}$ , the

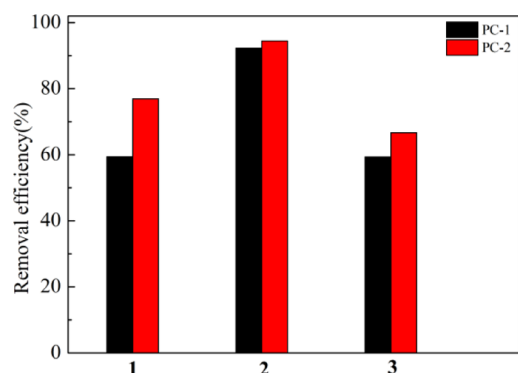


**Figure 13.** Removal efficiency of mesoporous carbon in Hg solution and removal efficiency of mesoporous carbon against in situ Hg from honeysuckle water decoction; (1)  $0.01 \text{ mg}\cdot\text{L}^{-1}$  Hg; (2)  $0.13 \text{ mg}\cdot\text{L}^{-1}$  Hg; (3) honeysuckle water decoction containing  $0.006 \text{ mg}\cdot\text{L}^{-1}$  of in situ mercury.

removal rates of in situ Hg in the honeysuckle by PC-1 and PC-2 could reach 59 and 66%, respectively. Compared with the mercury ion solution, PC-1 and PC-2 had lower removal rates of in situ mercury in the honeysuckle water decoction, which signifies that there exist some components in the honeysuckle water decoction itself that can occupy the active adsorption sites of mesoporous carbon, and that the ultra-low concentration Hg itself is difficult to be adsorbed due to few contact sites, resulting in lower adsorption efficiency. Furthermore, PC-2 has higher removal efficiency compared with PC-1, which may be because PC-2 has more adsorption sites or chelating groups than PC-1.

**2.4. Analysis of Chlorogenic Acid Content of HPLC Index Medicinal Component.** One of the main medicinal components of the honeysuckle extract is chlorogenic acid, and the “Pharmacopoeia of the People’s Republic of China” (2020 edition) stipulates that one of the index components in the honeysuckle extract is chlorogenic acid. Consequently, the effects of the standard solution of chlorogenic acid, honeysuckle water decoction, and honeysuckle water decoction after the removal of Hg using mesoporous carbons PC-1 and PC-2 were compared to determine the difference of peak area on the medicinal component (chlorogenic acid). The results are shown in Figure 14. From Figure 14, the retention time of chlorogenic acid standard (a) was 8.933 min, and the retention times of chlorogenic acid in honeysuckle water decoction (b), honeysuckle water decoction after Hg removal from PC-1 (c), and honeysuckle water decoction after Hg removal from PC-2 (d) were 8.958, 8.716, and 9.043 min, respectively, and the peak areas of chlorogenic acid were 12796.4, 11801.1, and 11492.7 mAu·min, respectively. The retention time of chlorogenic acid was basically consistent and the reduction of the peak area was smaller. These results indicate that the mesoporous carbons PC-1 and PC-2 have less effect on the adsorption of chlorogenic acid in water decoction of honeysuckle.

### 3. CONCLUSIONS

In conclusion, the removal of trace mercury (Hg) from honeysuckle water decoction with high efficiency was achieved via mesoporous carbon (PC-2) obtained by using sucrose as a

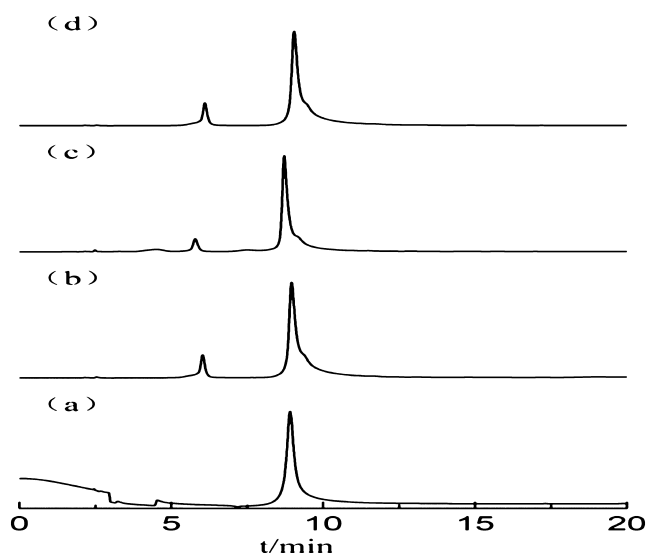


**Figure 14.** HPLC diagrams: (a) chlorogenic acid standard, (b) honeysuckle water decoction, (c) honeysuckle water decoction after Hg removal by PC-1, and (d) honeysuckle water decoction after Hg removal by PC-2.

carbon source and urea as a nitrogen source. A high specific surface area ( $1077.44 \text{ m}^2\cdot\text{g}^{-1}$ ) was observed for PC-2, which was functionalized for  $-\text{OH}/-\text{COOH}/-\text{NH}_2$ . Compared to PC-1 functionalized for  $-\text{OH}/-\text{COOH}/-\text{NH}_2$ , PC-2 was more efficient for mercury removal. It implies that nitrogen doping may contribute to the adsorption of mercury.

We obtained the best adsorption conditions for mercury by varying dosages, times, temperatures, and so on. The mesoporous carbon PC-2 synthesized with sucrose as the carbon source and urea as the nitrogen source had the highest Hg removal rate and reached equilibrium after 0.5 h. The removal rate of PC-2 was close to 100% under optimal conditions. An adsorption kinetic study reveals that the adsorption of Hg by PC-2 was better described by the pseudo-second-order kinetic model; whereas an adsorption isotherm study suggests that the adsorption process of Hg onto the PC-2 was better described by the Freundlich isotherm model. Combined with the structural characterization, it can be speculated that the process of adsorption of mercury ions onto PC-2 was mainly chemical adsorption. Further, the in situ removal rate of mercury ions from honeysuckle water decoction was 66%, which was higher than anything else tested so far, and there was little loss of active ingredient (chlorogenic acid). There is a potential for mesoporous carbon (PC-2) to remove trace mercury from honeysuckle water decoction.

## 4. EXPERIMENTAL SECTION

**4.1. Materials.** Formaldehyde (37 wt %), phenol, hydrochloric acid, nitric acid, and Pluronic F127 were purchased from Energy Chemical, Shanghai, China. Urea was purchased from Chengdu Pusi Biotechnology Co. LTD., Sichuan, China. Sucrose was purchased from Guilin Shunfeng Sugar Co. LTD., Guangxi, China. Chlorogenic acid standard was purchased from Beijing Soleibao Technology Co. LTD., China. Mercury content ( $0.009\text{--}0.011 \text{ mg}\cdot\text{kg}^{-1}$ ) in honeysuckle was determined by Guizhou Institute of Products Quality Inspection & Testing, Guiyang, China. The single element standard solution



of mercury ( $1000 \mu\text{g}\cdot\text{mL}^{-1}$ ) was purchased from the National Non-ferrous Metal and Electronic Materials Analysis and Testing Center, China. Deionized water was made in the laboratory. All the abovementioned chemicals were of analytical grade and commercially available.

**4.2. Preparation of Mesoporous Carbon.** The template method is a common method for preparing mesoporous carbon, which is mainly divided into hard template method and soft template method. Therefore, in the study, mesoporous carbons were prepared by soft and hard template methods, which were applied to honeysuckle extracts to investigate their feasibility and adaptability for high efficiency removal of trace mercury in honeysuckle water decoction. The specific synthesis methods are as follows.

**4.2.1. Soft Template Method.** 6 g of phenol, 21 mL of formaldehyde solution (37%), and 90 mL ( $0.1 \text{ mol}\cdot\text{L}^{-1}$ ) of sodium hydroxide solution were placed in a flask and stirred at  $70^\circ\text{C}$  for 0.7 h. Then 0.80 g of Pluronic F127 was dissolved in 20 mL of deionized water and slowly poured into the abovementioned solution and stirred at  $70^\circ\text{C}$  for 3 h. Next, 50 mL of deionized water was added to dilute the solution. When solids were observed floating on the surface in the reaction solution, after waiting for a few minutes, and the reaction was shut down. The obtained solution was cooled to room temperature; the upper solid layer was primary carbon. The obtained primary carbons were calcined at  $900^\circ\text{C}$  for 1 h with a heating rate of  $5^\circ\text{C}/\text{min}$  in a nitrogen flow. The mesoporous carbons (PC-1) were obtained by dissolution of the soft template in 6 M hydrochloric acid ethanol solution at  $70^\circ\text{C}$  for 12 h, isolated by filtration, washed with distilled water until the pH did not change, and dried at  $60^\circ\text{C}$ .

**4.2.2. Hard Template Method.** Sucrose and concentrated nitric acid mixed in a mass ratio of 5:1 were placed in a surface dish, and they were laid for about 3–4 days. Next, the mixture was heated in a vacuum drying oven at  $160^\circ\text{C}$  for 2–3 h; it was then taken out and ground finely after cooling; and then, 1/2 sucrose amount of urea and nano-magnesium oxide were mixed with the abovementioned mixture again. The mixing was followed by the carbonization at  $800^\circ\text{C}$  for 2 h with a heating rate of  $5^\circ\text{C}/\text{min}$  under a  $\text{N}_2$  atmosphere in a tubular furnace. Finally, the mesoporous carbon (PC-2) was refluxed with concentrated nitric acid at room temperature for 24 h, isolated by filtration and washed with distilled water until the pH did not change, and dried at  $100^\circ\text{C}$ .

**4.3. Characterization.** The morphologies of mesoporous carbon were observed by scanning electron microscopy (SEM, Zeiss-Sigma300, Zeiss, Germany) and transmission electron microscopy (TEM, Axio Scope AI A, Zeiss, Germany). The chemical composition was determined by Fourier Transform infrared spectroscopy (FT-IR, Vertex70, Bruker, Germany) and X-ray photoelectron spectroscopy (XPS, ESCALAB Xi<sup>+</sup>, Thermo Scientific, USA). The specific surface area and pore structure were determined by a specific surface area analyzer (JW-BK122W, Beijing, China).

**4.4. Experiment on Mercury Adsorption.** The mesoporous carbon was placed in various Hg concentrations and then fixed in a water bath thermostatic oscillator and shaken for a certain time until the adsorption equilibrium; the solution pH was adjusted by 0.1 M HCl and 0.1 M NaOH. After reaction, the mesoporous carbon was separated from the solution and filtered through a  $0.22 \mu\text{m}$  membrane filter. The Hg concentrations were measured by inductively coupled plasma mass spectrometer (ICP-MS, iCAP6300MFC, Thermo

Fisher, USA). Then the average value was taken three times in parallel to calculate the removal efficiency ( $E$  (%)). The removal rate of Hg is calculated as follows.

$$E(\%) = \frac{C_0 - C_e}{C_0} \times 100\% \quad (5)$$

where  $C_0$  ( $\text{mg}\cdot\text{L}^{-1}$ ) and  $C_e$  ( $\text{mg}\cdot\text{L}^{-1}$ ) were the initial concentration and adsorption equilibrium concentration of Hg solution, respectively.


**4.5. Removal of Mercury from Honeysuckle Water Decoction.** Honeysuckle powder (1 g) was mixed with 50 mL of deionized water and then extracted for 30 min. The water decoction was filtered, and deionized water was added for confirming the concentration. Then 5 mg of PC-1 or PC-2 was added to 20 mL of honeysuckle water decoction and left to a thermostatic oscillator (DF-101S, Shanghai, China) at  $30^\circ\text{C}$  for 420 min or 30 min; other conditions were kept constant. The subsequent mixtures were separated by a Nylon  $0.22 \mu\text{m}$  syringe filter. Samples were then determined via ICP-MS, and then, the removal efficiency was calculated.

**4.6. Effect of Mesoporous Carbon on the Pharmacodynamic Component (Chlorogenic Acid) of Honeysuckle Water Decoction.** Mesoporous carbons PC-1 and PC-2 were mixed with the water decoction of honeysuckle after a mild agitation of 108 rpm for 30 and 420 min at  $30^\circ\text{C}$ . Then, the mixed solutions were filtered with a  $0.22 \mu\text{m}$  filter membrane and sent for HPLC analysis. The reference solution and the samples were subjected to HPLC (Agilent 1260, USA) to estimate the effects of mesoporous carbon PC-1 and PC-2 on the active ingredients of honeysuckle. The standard substance of chlorogenic acid was resolved in 50% methanol to prepare the reference solution<sup>47</sup> ( $0.0535 \text{ mg}\cdot\text{mL}^{-1}$ ). The chromatographic conditions were as follows: ZORBAX SB-C18 column ( $4.6 \times 250 \text{ mm } 5 \mu\text{m}$ ) with a room temperature, acetonitrile–0.5% glacial acetic acid solution as the mobile phase with a gradient elution, and 1 mL/min flow rate with a detection wavelength of 326 nm.

## AUTHOR INFORMATION

### Corresponding Authors

Jiayong Zhang – College of Pharmacy, Zunyi Medical University, Zunyi 563000, China;  
Email: zhangjiayong2006@126.com

Ming Yu – College of Pharmacy, Zunyi Medical University, Zunyi 563000, China;  orcid.org/0000-0001-5060-4249;  
Email: Cosmosym920@163.com

### Authors

Wenjie Lu – College of Pharmacy, Zunyi Medical University, Zunyi 563000, China; Institute of Basic Theory of Chinese Medicine, China Academy of Chinese Medical Sciences, Beijing 100700, China

Yiqian Ma – Guizhou Institute of Products Quality Inspection & Testing, Guiyang 550016, China

Huanyu Lu – Guizhou Institute of Products Quality Inspection & Testing, Guiyang 550016, China

Xiaoyan Yuan – College of Pharmacy, Zunyi Medical University, Zunyi 563000, China

Complete contact information is available at:  
<https://pubs.acs.org/10.1021/acsomega.2c05863>

## Author Contributions

W.L. and M.Y. conceived and designed the experiments. W.L. and Y.M. performed the experiments. W.L., Y.M., and M.Y. analyzed the data and wrote the manuscript. Other authors also contributed to the conduction of the experiment and the writing of the manuscript. All authors have read and approved the final version of the manuscript.

## Notes

The authors declare no competing financial interest.

## ACKNOWLEDGMENTS

This study was supported by the Special project for academic seedling cultivation and innovation exploration in Guizhou Province of China (Talent (2018) 5772-034) and the Science and Technology Talent Training Program in Zunyi City (Zunyi Science and Technology branch [2021]283 and [2020-009]).

## REFERENCES

- (1) Xia, L.; Zhang, B.; Gong, Z.; Deng, Q. Research progress on preparation of amino-terminated hyperbranched polymer graft bagasse cellulose and on its adsorption properties of heavy metal ions. *J. Food Saf. Food Qual.* **2014**, *5*, 3035–3041.
- (2) Liu, C.; Qin, J.; Dou, X.; Yang, M.; Sun, X. Extrinsic harmful residues in Chinese herbal medicines: types, detection, and safety evaluation. *Chin. Herb. Med.* **2018**, *10*, 117–136.
- (3) Yang, L.; Zhang, Y.; Wang, F.; Luo, Z.; Guo, S.; Strähle, U. Toxicity of Mercury: Molecular Evidence. *Chemosphere* **2020**, *245*, 125586.
- (4) Liang, Q.; Li, R.; Liu, S. Progress of Reducing Heavy Metal Content in Chinese Medicine. *J. Trace Elem. Health Res.* **2012**, *29*, 48–50.
- (5) Liang, H.; Chen, S.; Liu, G.; Hou, X. Study on the Removal of Lead, Cadmium and Copper from the Decoction of Radix isatidis by Macroporous Resin (D751) Column. *J. Anhui Agric. Sci.* **2012**, *40* (4), 2144–2146, DOI: 10.13989/j.cnki.0517-6611.2012.04.046.
- (6) Shu, G.; Zheng, Q.; Chen, L.; Jiang, F.; Dai, C.; Hui, Y.; Du, J. Screening and identification of Lactobacillus with potential cadmium removal and its application in fruit and vegetable juices. *J. Food Control* **2021**, *126*, 108053.
- (7) Ren, Y.; Sun, M.; Peng, H.; Huang, K. Removal of heavy metals from extract of *Angelica sinensis* by EDTA-modified chitosan magnetic adsorbent. *China J. Chin. Mater. Med.* **2013**, *38*, 3709–3712.
- (8) Tang, F.; Ni, Z.; Liu, Y.; Yu, Z.; Wang, R.; Mo, R. Arsenic Speciation in Honeysuckle (*Lonicera japonica* Thunb.) from China. *J. Biol. Trace Elem. Res.* **2015**, *168*, 269–275.
- (9) Ni, Z.; Yu, Q.; Liu, Y.; Tang, F. Identification of Geographical Origin of Honeysuckle (*Lonicera Japonica* Thunb) by Discriminant Analysis Using Rare Earth Elements. *J. Anal. Lett.* **2016**, *49*, 2312–2321.
- (10) Song, Y.; Wang, H.; Ni, F.; Wang, X.; Zhao, Y.; Huang, W.; Wang, Z.; Xiao, W. Study on anti-inflammatory activities of phenolic acid from *Lonicerae Japonicae* Flos. *J. Chin. Tradit. Herb. Drugs* **2015**, *46*, 490–495.
- (11) Xiao, Z.; Xie, M.; Gan, L.; Fang, M.; Zhou, X.; Zhou, Y.; Wei, H.; Chen, H.; Huang, J.; Pharmacy, S. Determination of chlorogenic acid, total flavonoids and antioxidant activity in Flos *Lonicerae Japonicae* and Flos *Lonicerae*. *J. Chin. Tradit. Herb. Drugs* **2019**, *50*, 210–216.
- (12) Wang, X.; Liu, J.; Xie, Z.; Rao, J.; Xu, G.; Huang, K.; Li, W.; Yin, Z. Chlorogenic acid inhibits proliferation and induces apoptosis in A498 human kidney cancer cells via inactivating PI3K/Akt/mTOR signalling pathway. *J. Pharm. Pharmacol.* **2019**, *71*, 1100–1109.
- (13) Guo, L.; Zhou, L.; Wang, S.; Kang, C.; Hao, Q.; Yang, W.; Zhou, L.; Li, Z.; Ma, Z.; Huang, L. Statistic and Analysis of Heavy Metal residues of Chinese crude drug with International Standard of

Chinese Medicine-Chinese Herbal Medicine Heavy Metal. *Sci. Technol. Rev.* **2017**, *35*, 91–98.

(14) Li, Y.; Liu, Z.; Huang, J.; Zhang, Y.; Li, Q. Research progress on heavy metals removal from plant extracts. *J. Chin. Tradit. Herb. Drugs* **2019**, *50*, 1727–1733.

(15) Mo, J.; Liu, L.; Chen, L.; Fu, J.; Lv, X. Removal of Arsenic from aqueous extract of *Rehmannia Redix* using resin. *Chin. J. Mod. Appl. Pharm.* **2014**, *031*, 1190–1194.

(16) Yu, J.; Tang, Y.; Zhang, Y.; Xu, H.; Fan, M.; Wang, P. Preparation of adsorbents for selectively removal of heavy metals from *Salvia miltiorrhiz* extract. *J. Chin. Tradit. Herb. Drugs* **2018**, *49*, 1068–1074.

(17) Xiao, Q.; Han, J.; Jiang, C.; Luo, M.; Zhang, Q.; He, Z.; Hu, J.; Wang, G. Novel Fusion Protein Consisting of Metallothionein, Cellulose Binding Module, and Superfolder GFP for Lead Removal from the Water Decoction of Traditional Chinese Medicine. *J. ACS Omega* **2020**, *5*, 2893–2898.

(18) Wang, J.; Zheng, S.; Shao, Y.; Liu, J.; Xu, Z.; Zhu, D. Amino-functionalized Fe<sub>3</sub>O<sub>4</sub>@SiO<sub>2</sub> core-shell magnetic nanomaterial as a novel adsorbent for aqueous heavy metals removal. *J. Colloid Interface Sci.* **2010**, *349*, 293–299.

(19) Jiang, W.; Su, H.; Tan, T. Adsorption properties for heavy metal ions of molecular imprinting chitosan-coated diatomite beads in water-extraction liquid of *Rhodiola L.* *J. Chem. Ind. Eng.* **2008**, *59*, 1179–1183.

(20) Ao, M.; Yu, L.; Shi, Z.; Tao, Z.; Tang, B.; Shi, H. Method for Removing Ginkgolic Acid and Heavy Metals in Ginkgo Biloba Extract by Using Nanometer Material. CN 103110671 A, China, 2013. patent

(21) Zhang, X.; Wang, J.; Tong, Y.; Li, Y.; Ma, Z.; Wang, L. Application and Prospect of Macroporous Resin Technology in Extraction and Purification of Traditional Chinese Medicine. *Chin. J. Exp. Tradit. Med. Formulae* **2012**, *18*, 286–290.

(22) Zhang, S.; Liu, L.; Guo, H.; Xu, Y.; Gao, X. Technology adaptability research on removal of heavy metals in *Acanthopanax senticosus* extract with alkyl thiourea functionalised silica. *J. Chin. Tradit. Herb. Drugs* **2017**, *48*, 1561–1570.

(23) Ren, Y.; Abbood, H.; He, F.; Peng, H.; Huang, K. Magnetic EDTA-modified chitosan/SiO<sub>2</sub>/Fe<sub>3</sub>O<sub>4</sub> adsorbent: Preparation, characterization, and application in heavy metal adsorption. *Chem. Eng. J.* **2013**, *226*, 300–311.

(24) Nejadshafiee, V.; Islami, M. Adsorption capacity of heavy metal ions using sulfone-modified magnetic activated carbon as a bio-adsorbent. *J. Mater. Sci. Eng.* **2019**, *101*, 42–52.

(25) Kong, D.; Wang, R.; Guo, Y.; Li, X.; Yang, S.; Yang, M. Study on Simultaneous Removal of Heavy Metals Cadmium, Lead and Mercury in Xiaochaihu Decoction Compound Preparation by Bionic Materials. *J. Modernization of Traditional Chinese Medicine and Materia Medica-World Science and Technology* **2020**, *22*, 353–361.

(26) Liu, J.; Wickramaratne, N.; Qiao, S.; Jaroniec, M. Molecular-based design and emerging applications of nanoporous carbon spheres. *Nat. Mater.* **2015**, *14*, 763–774.

(27) Li, W.; Liu, J.; Zhao, D. Mesoporous materials for energy conversion and storage devices. *Nat. Rev. Mater.* **2016**, *1*, 16023.

(28) Lian, Q.; Yao, L.; Uddin Ahmad, A.; Gang, D.; Konggindinata, I.; Gallo, A.; Zappi, E. Enhanced Pb(II) adsorption onto functionalized ordered mesoporous carbon (OMC) from aqueous solutions: the important role of surface property and adsorption mechanism. *Environ. Sci. Pollut. Res. Int.* **2020**, *27*, 23616–23630.

(29) Barquilha, C.; Cossich, E.; Tavares, C.; Silva, E. Biosorption of nickel(II) and copper(II) ions in batch and fixed-bed columns by free and immobilized marine algae *Sargassum* sp. *J. Clean. Prod.* **2017**, *150*, 58–64.

(30) Zhang, Q.; Wang, R.; Liu, J.; Wu, J.; Xia, L.; Cui, X.; Bu, D. Preparation, characterization and application of mesoporous carbon materials derived from MgO template for removal of heavy metals. *Appl. Chem. Ind.* **2019**, *48*, 816–819.

(31) Zhang, W.; Yu, B.; Hu, Q. Preparation and pore structure control of resorcinol-formaldehyde resins-based monolithic hierarchical porous carbon. *Mater. Sci. Technol.* **2018**, *26*, 51–58.

- (32) Li, Z.; Wu, L.; Rao, W.; Tong, K.; Zhang, Q.; Zhang, J.; Liu, Y.; Liu, J.; Shu, S.; Xu, J. Synthesis and structural characterization of iron-modified phenolic resin. *Polym. Mater. Sci. Eng.* **2019**, *35*, 70–74.
- (33) Liu, Y.; Zhao, Q.; Cheng, G.; Xu, H. Exploring the mechanism of lead(II) adsorption from aqueous solution on ammonium citrate modified spent *Lentinus edodes*. *Chem. Eng. J.* **2011**, *173*, 792.
- (34) Srivastava, S.; Agrawal, S.; Mondal, M. Characterization, isotherm and kinetic study of *Phaseolus vulgaris* husk as an innovative adsorbent for Cr(VI) removal. *Kor. J. Chem. Eng.* **2016**, *33*, 567–575.
- (35) Li, H.; Wang, Y.; Xu, T.; Zhu, M.; Xu, Y.; Wu, J. Preparation of sucrose-based carbon material by the hydrothermal carbonization method. *J. Journal of Qiqihar University (Natural Science Edition)* **2018**, *34*, 47–49.
- (36) Yu, M. *Study on Controllable Preparation and Properties of Coal Tar-based Foam Carbon*; D. Guizhou University, 2019.
- (37) Zheng, X.; Lv, W.; Tao, Y.; Shao, J.; Zhang, C.; Liu, D.; Luo, J.; Wang, D.; Yang, Q. Oriented and Interlinked Porous Carbon Nanosheets with an Extraordinary Capacitive Performance. *Chem. Mater.* **2014**, *26*, 6896–6903.
- (38) Zhou, Q. Q.; Chen, X. Y.; Bo, W. An activation-free protocol for preparing porous carbon from calcium citrate and the capacitive performance. *Microporous Mesoporous Mater.* **2012**, *158*, 155–161.
- (39) Zhuang, H.; Cao, L.; Dai, L.; Yin, H.; Wang, J.; Aikebaier, R. Preparation of sulfurized poly (m-aminothiophenol)/starch composite material and its adsorption of Hg(II). *Polym. Bull.* **2022**, *35* (3), 54–62, DOI: 10.14028/j.cnki.1003-3726.2022.03.007.
- (40) Mudasir, M.; Karelius, K.; Aprilita, A.; Wahyuni, W. Adsorption of mercury(II) on dithizone-immobilized natural zeolite. *J. Environ. Chem. Eng.* **2016**, *4*, 1839–1849.
- (41) Huang, J.; Song, W.; Yao, Z. Pb (II) adsorption from water onto polyacrylic acid/chestnut shell pigment hydrogel. *J. Southwest For. Univ.* **2023**, *43* (6), 1–9.
- (42) Erdem, B.; Özcan, A.; Gök, O.; Özcan, A. Immobilization of 2,2'-dipyridyl onto bentonite and its adsorption behavior of copper(II) ions. *J. Hazard Mater.* **2009**, *163*, 418–426.
- (43) Fogarty, R. V.; Tobin, J. M. Fungal melanins and their interactions with metals. *Enzym. Microb. Technol.* **1996**, *19*, 311–317.
- (44) Yang, T.; Xu, Y.; Huang, Q.; Sun, Y.; Liang, X.; Wang, L.; Qin, X.; Zhao, L. Adsorption characteristics and the removal mechanism of two novel Fe-Zn composite modified biochar for Cd(II) in water. *Bioresour. Technol.* **2021**, *333*, 125078.
- (45) Pan, Y.; Yan, S.; Tang, X.; Wang, Q.; Wang, X.; Yang, J. Preparation of coal gangue microspheres and its adsorption properties of methyl violet and malachite green in waste water. *J. Funct. Mater.* **2018**, *49*, 06001–06008.
- (46) Yang, J.; Zhang, Y.; Yang, D.; Liu, M. Adsorption Characteristics of Pb<sup>2+</sup> on Rice Straw. *Res. Environ. Sci.* **2012**, *25*, 815–819.
- (47) Qu, M.; Cheng, Y.; Cao, C.; Li, G. Determination of content of chlorogenic acid in honeysuckle by HPLC. *Food Res. Dev.* **2015**, *36*, 145–147.